Stony Brook University

Synthesis, Characterization and Luminescence Studies of Lanthanide-2,5-Thiophenedicarboxyalate Frameworks

A Thesis Presented

by

Quddus Amin Nizami

to

The Graduate School

in Partial Fulfillment of the

Requirements

for the Degree of

Master of Science

in

Chemistry

Stony Brook University

December 2011

Stony Brook University

The Graduate School

Quddus Amin Nizami

We, the thesis committee for the above candidate for the

Master of Science degree, hereby recommend

acceptance of this thesis.

John B. Parise, Advisor
Distinguished Professor, Department of Geosciences and Chemistry

Peter Khalifah, Chair
Assistant Professor, Department of Chemistry

Alexander Orlov, Third Member
Assistant Professor, Department of Materials Science and Engineering

This thesis is accepted by the Graduate School

Lawrence Martin
Dean of the Graduate School

Abstract of the Thesis

Synthesis, Characterization and Luminescence Studies of Lanthanide-2,5-Thiophenedicarboxyalate Frameworks

By

Quddus Amin Nizami

Master of Science

in

Chemistry

Stony Brook University

2011

Four novel three-dimensional lanthanide-thiophenedicarboxylate hybrid compounds, $Tb_4(C_{44}S_6O_{37})$ [Tb_4(2,5-TDC) **[1];** TDC= thiophenedicarboxylate]; space group ***P-1***, a=12.8068(9) Å, b=14.5574(10) Å, c= 19.1276(12) Å, α= 106.660(2)°, β= 105.621(2)°, γ= 93.691(2)°, V= 3251.21(4) $Å^3$, $Dy_4(C_{46}H_{43}O_{32}S_6)$ [Dy_4(2,5-TDC) **[2]**], space group ***P-1***, a= 12.807(8) Å, b= 14.6904(9) Å, c= 19.0866(11) Å, , α= 107.101(1)°, β= 105.534(1)°, γ= 93.529(2)°, V= 3266.9(3) $Å^3$, $Nd_2(C_{21}O_{16}S_4)$ [Nd_2 (2,5-TDC) **[3]**], space group ***C***2/c, a=24.037(2) Å, b=10.0649(8) Å, c=17.963(3) Å, α=90°, β=128.656(2)°, γ= 90°, V=3393.8(7) $Å^3$ and $Er_2(C_{45}O_{32}S_6)$ **[**Er_2 (2,5-TDC) **[4]**], space group ***Pbam***, a=20.9870(15) Å, b=17.1420(12) Å, c=19.2961(14) Å, α=90°, β=90°, γ= 90°, V= 6942.0(9) $Å^3$ were synthesized. Compounds **1**, **2**, and **4** are formed

ethanol-water mixtures as solvent, while compound **3** is formed using only ethanol. All reactions take place at 105°C. Luminescent properties, thermo gravimetric analyses (TGA), and powder x-ray diffraction (PXRD) of these complexes have also been studied. Compounds were excited at 397 nm and Tb_2 $(TDC)_3$ shows the most intense emission of the four compounds. These findings offer a better understanding of how linker choice can affect the luminescent properties of resulting coordination networks.

Dedication

I dedicate my thesis work to my loving father, Muhammad Amin Nizami and mother, Begum Taj Amin.

Table of Contents

List of Figures

List of Abbreviations

MOFs – Metal Organic Frameworks

TDC – 2,5-thiophene dicarboxylic acid

PXRD – Powder X-ray Diffraction

TGA – Thermogravimetric Analysis

CN – Coordination Network

DOE – Department of Energy

SBU – Secondary Building Unit

UV – Ultra Violet

NIR – Near-Infrared

MLCT – Metal-to-Ligand Charge Transfer

LMCT – Ligand-to-Metal Charge Transfer

ITQMOF – Instituto de Technologia Metal Organic Frameworks

Ln – Lanthanide

ISC – Inter-system crossing

ET – Energy Transfer

BU – Building Unit

PL – Photoluminescence

1D – One Dimensional

2D – Two Dimensional

3D – Three Dimensional

Acknowledgments

I would like to thank **Prof. John Parise** for giving me the opportunity to work in his laboratory as research project assistant to earn my Master's degree in Chemistry while providing the guidance and support through difficult times. I would like to give my gratitude to *John Parise* for his supervision, advice, and guidance from the very early stage of this research as well as giving me extraordinary experiences throughout the work.

I would also like to thank and gratefully acknowledge **Debasis Banerjee** and **Paul Calderone** for their advice, supervision, and crucial contribution which made them backbone of this research and this thesis. *Debasis and Paul*, I am grateful in every possible way and hope to keep up our collaboration in future. I would like to thanks to all the members of *Parise* group along my master's research work.

I would also like to thank my committee members, Chairperson Professor *Peter Khalifah* and Professor *Alexander Orlov* for their support during the M.S. defense.

Special thanks should also be given to my family and friends for which without their help and support, I would not be where I am today.

Lastly, I offer my regards and blessings to all of those who supported me in any respect during the completion of the project.

I. INTRODUCTION:

Overview and Design of Metal Organic Frameworks (MOFs)

Metal-organic frameworks (MOFs) are a class of hybrid materials that have attracted much attention in materials chemistry due to their fascinating structural topologies, and because their micro porous properties potentially make them suitable for such applications as gas sorption and separation[1]. MOFs exist as infinite crystal lattices with metal nodes connected by organic molecules with at least two functional groups (figure 1).

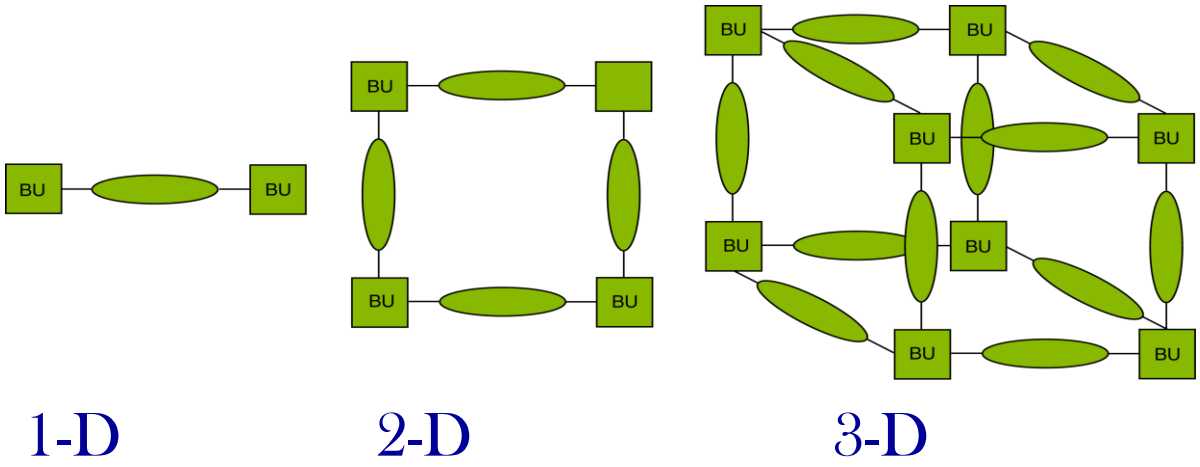

Figure 1 MOFs with various dimensionalities (Diagram courtesy of Lauren Borkowski)

The number of papers that feature the term "coordination polymers", or "metal-organic frameworks" has increased dramatically over the past decade, indicating the design and synthesis of extended coordination materials has been an area of intense research and great challenge for

materials chemists. The diversity of structures and topologies reported result from variation a number of factors, such as the nature of the ligand, metal center, and synthetic conditions. Specifically, the number of functional groups and the stereochemistry of the organic linker, the nature of the solvent, coordination preferences of the metal ion, and reaction temperature can also affect the MOF produced. How systematic manipulation of synthetic parameters, for a given composition , leads to novel coordination networks, is illustrated in the work of Forster et al.[2], who reported a series of structures (figure 2) resulting from changes in only one variable, synthesis temperature.

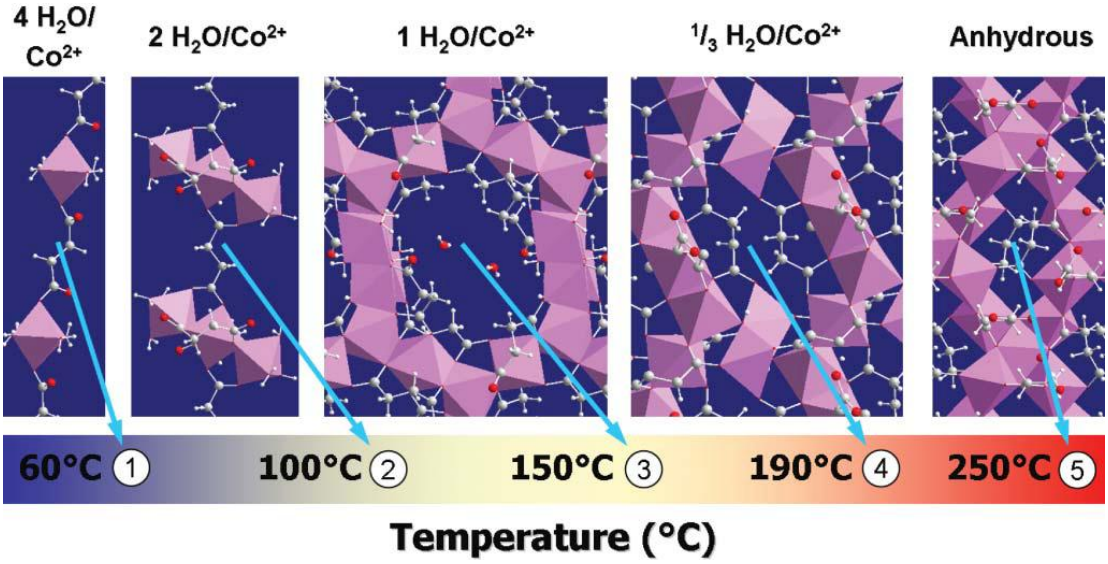

Figure 2 Demonstration of solvent water incorporation control with varying temperature under hydrothermal conditions.[2]

The preference of a particular metal center for a specific geometry and coordination environment further affects the resulting coordination network (CN) structure. As an illustration,

Zhang, et al.[3] synthesized the compound [Cu_2 (4,4'-bipy)$_4$] (D-HCam) (4,4'-bipy)^2.12H_2O, where the Cu^{2+} metal centers adopt a tetrahedral coordination geometry which contributes to the overall diamondoid network via 4.4'-bipyridine linkages as shown in figure 3.

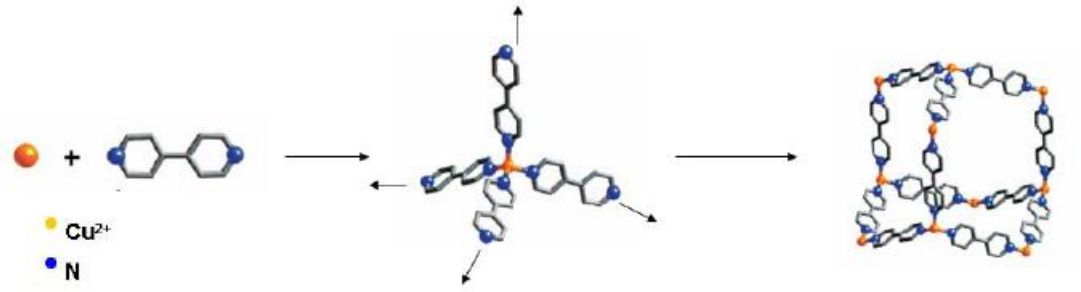

Figure 3 Cu^{2+} ion in [Cu_2 (4,4'-bipy)$_4$] (D-HCam) (4,4'-bipy)$_2$.12H_2O adopts a tetrahedral geometry and extended into a diamondoid network via 4.4'-bipyridine linkages. Counter Anions and solvents of crystallization removed for clarity.

By Comparison, Liu et al.[4], synthesized the compound [Cd (4 4'-bpy)$_2$(H_2O)$_2$](ClO_4)$_2$ 1.5(4,4'-bpy)], where the Cd^{2+} metal centers adopts the octahedral geometry shown in figure 4. In the octahedron, the axial positions are occupied by terminal water molecules while 4, 4'-bipyridine molecules link to the metal centers at the equilateral positions. A square net is formed in the extended framework due to the geometry around the metal center.

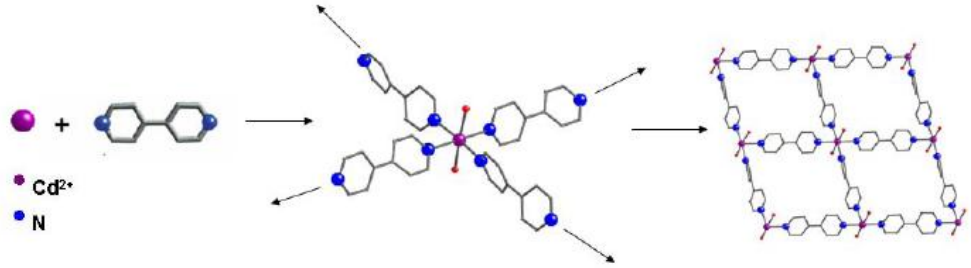

Figure 4 Cd^{2+} [$Cd(4,4'\text{-bpy})_2(H_2O)_2](ClO_4)_2$ 1.5(4,4'-bpy)] adopts an octahedral geometry by binding to two water molecules (red=oxygen atoms) and four 4,4'-bipridine molecules. Hydrogen, counter anions, and solvents of crystallization removed for clarity.

Potential Applications of MOFs

Potential applications of MOFs include catalysis,[5] optics,[6] electronics,[7] gas storage,[8] separation science,[9] and luminescence.[10] Because of the DOE's ambitious target of 9 wt. % by 2015 for materials capable of storing hydrogen for transport applications, the capture and release of fuel (H_2, CH_4) and waste (CO_2) gases is a widely researched application of MOFs[11]. MOFs were thought to be good candidates to meet these goals because of their large surface areas, tunability of pore size, and adsorption properties. For an illustration, Yaghi has reported many MOFs based on the $[Zn_4O]_{6+}$ secondary building unit (SBU) which are effective at storing H_2. The most famous of these frameworks, MOF-5 is shown in figure 5.[12]

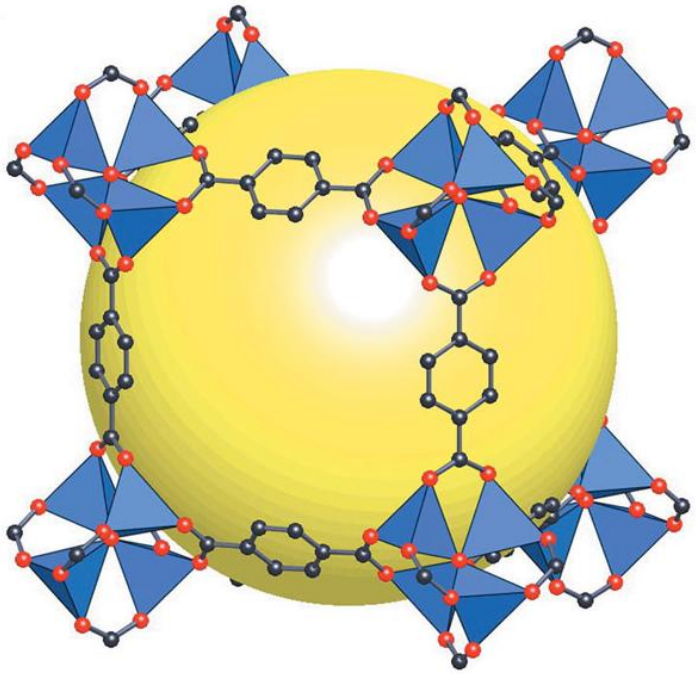

Figure 5 MOF-5[12] the yellow sphere represents the larger sphere that can occupy the pore without contacting the van der Waals frameworks.

Some MOFs are also excellent candidates for catalysis because of their regular structural nanoporosity; a size in between aluminosilicate zeolites (0.4 - 1 nm) and surface metal- organic catalyst technologies. For example, in 2005, Lin reported the compound $[Cd_3C_{l6}L_3]$ (L =(*R*)-6,6´-dichloro-2,2´-dihydroxy-1,1´-binapthyl-4,4´-bipyridine), which was highly porous homochiral MOF (1.6 nm). This material was used to catalyze the enantioselective addition of diethylzinc to aromatic aldehydes.[13]

II. CONCEPTS OF LUMINESCENCE:

Luminescence is defined as emission of light due to the relaxation of electrons that have been stimulated by the absorption of energy. Excitation energy can be generated in the form of electric fields or ionizing radiation. The two basic types of luminescence are fluorescence and phosphorescence. Fluorescence refers to the emission of light between energy states of spin-allowed transitions (i.e., singlet-to-singlet emission), and has typical lifetimes last no more than 10 ns. Conversely, phosphorescence is spin-forbidden transition (i.e., triplet-to-singlet emission) and has lifetimes that can be as long as several seconds. Allowed and forbidden transitions are due to quantum mechanical probabilities where in forbidden transition, the excited state electrons don't follow the relaxation path of least resistance. The schematic shown in Figure 6, known as a Jablonski diagram[14], is drawn to represent the electronic structure typical of organic luminophores.

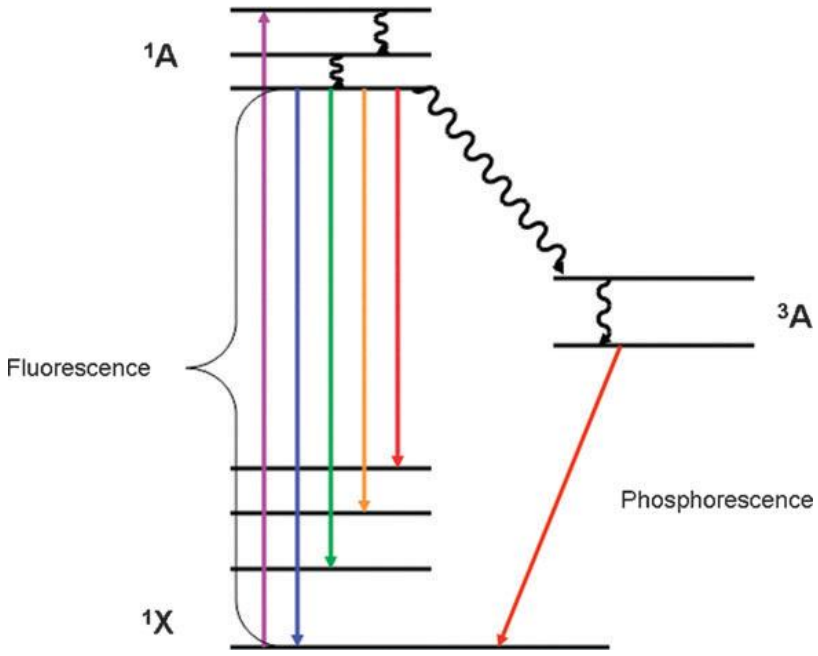

Figure 6 Jablonski diagram displaying schematically the electronic states of the organic linker involved in luminescence phenomena[20]

The conjugated organic linker excitation usually occurs through the allowed singlet–singlet transition and most of the emission occurs from the lowest singlet excited state (1A), unless efficient non-radiative is transferred to lower-lying triplet state (3A). Luminescence in lanthanide ions follows various Laporte selection rules (no change of parity from the ground state to the excited state), often leading to weak and long-lived emission that could be termed as phosphorescence which is spin-forbidden. The distance in the electronic state between the ground and excited states of the absorbing species is referred to the Stokes Shift, which causes the difference between the excitation and emission maxima. When a molecule or atom absorbs light, it enters an excited electronic state. The Stokes shift occurs because the molecule loses a small amount of the absorbed energy before re-releasing the rest of the energy as fluorescence depending on the time between the absorption and the re-emission. Stokes fluorescence is the

reemission of longer wavelength (lower frequency) photons (energy) by a molecule that has absorbed photons of shorter wavelengths. Both absorption and radiation of energy are unique characteristics of a particular molecule or structure during the fluorescence process. Light is absorbed by molecules in about 10-15 seconds which causes electrons to become excited to a higher electronic state. The electrons remain in the excited state for about 8-10 seconds then, assuming all of the excess energy is not lost by collisions with other molecules, the electron returns to the ground state. Energy is given off in order for the electrons to fall back to their ground state. Emitted light always has a longer wavelength than the absorbed light due to limited energy loss by the molecule prior to emission.

III. LANTHANIDE LUMINESCENCE AND MOFS:

For the last decade, research has focused on several potential applications of luminescent lanthanide ions: such as (a) to use in the lighting industry for the engineering of lamp phosphors, (b) to provide electroluminescent materials for organic light emitting diodes and optical fibers for telecommunications, and (c) to yield functional complexes for biological assays and medical imaging purposes.[15]

The trivalent ions of the lanthanide series are characterized by a gradual filling of the 4f orbitals, from $4f^0$ (for La^{3+}) to $4f^{14}$ (for Lu^{3+}) and their electronic configuration generate a variety of electronic configuration with different energy band levels as shown in figure 7[16]. These electronic energy levels are well defined due to the shielding of the 4f orbitals by the filled

$5s^2 5p^6$ subshells. However, each lanthanide ion exhibits narrow and characteristic 4f–4f transitions. All Ln^{3+} ions except La^{3+} and Lu^{3+} can generate luminescent *f-f* emissions from ultraviolet (UV) to visible and near-infrared (NIR) light. For decades, a well-known strategy to generate highly luminescent sensors has been to incorporate lanthanide ions into materials. Ions such as Eu^{3+}, Tb^{3+}, Sm^{3+}, and Tm^{3+} emit red, green, orange, and blue light, respectively, while the Yb^{3+}, Nd^{3+}, and Er^{3+} (NIR) luminescence, and still other lanthanide ions (Pr^{3+}, Sm^{3+}, Dy^{3+}, Ho^{3+}, and Tm^{3+}) also shows transitions in the NIR region. Gd^{3+} emits in the UV region and its luminescence can be observed in the absence of organic ligands due to its low-lying singlet and triplet state[17]. Eu^{3+} and Tb^{3+} are the lanthanide ions which are most commonly used in sensing applications due to their strong visible luminescence in the red and green region, respectively.

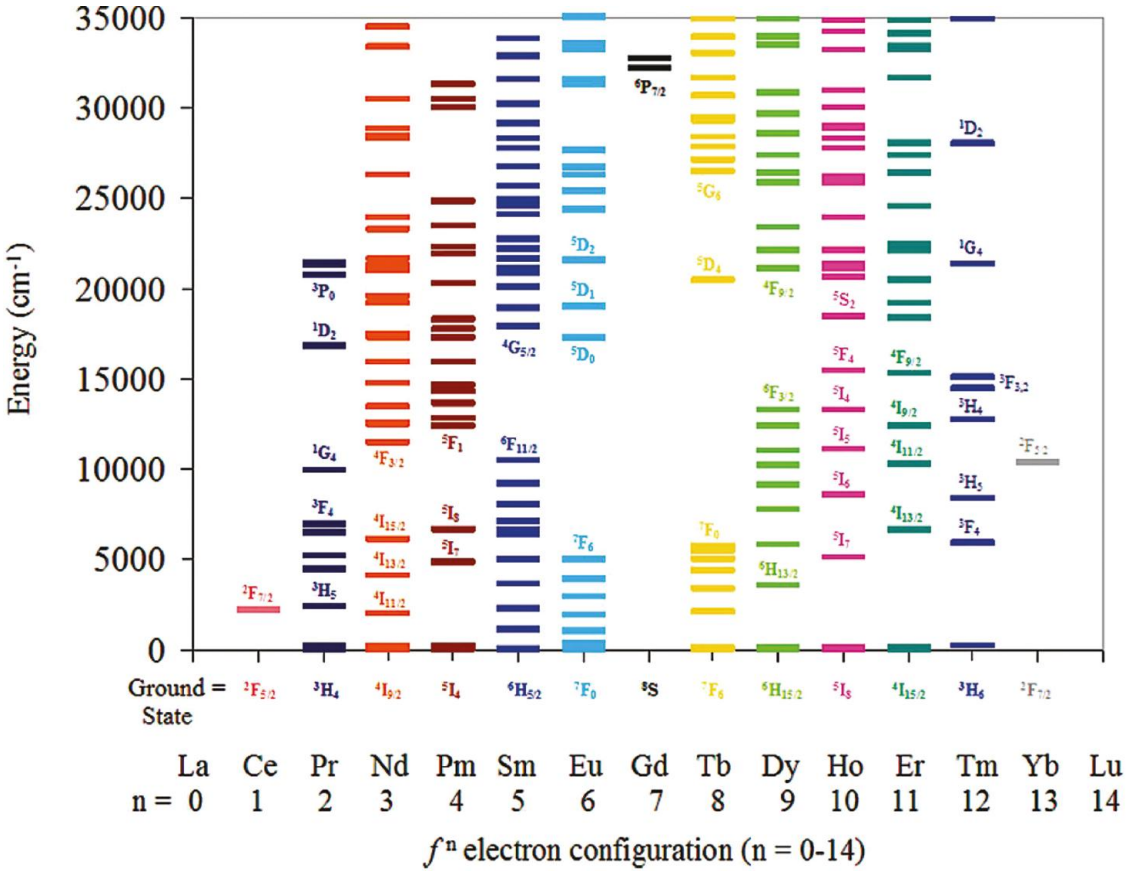

Figure 7 Electronic excited-state energy levels for Ln^{3+} ions

Hybrid materials are very promising as multifunctional luminescent materials because of their inorganic and organic moieties can each express or amplify the characteristics luminescent. Metal-to- ligand charge transfer (MLCT) and ligand-to-metal charge transfer (LMCT) within metal organic frameworks (MOFs) are good examples of hybrid materials can provide additional luminescent functionalities[18]. Metal-organic frameworks are a platform to develop solid state luminescent materials due to their well- defined environments for luminophores in crystalline form. Traditional inorganic and organic luminescent materials have been explored extensively for their diverse functionalities as well as applications in lighting, display, and optical devices[19].

Metal organic frameworks that possess luminescent properties together with size and shape-selective sorption properties can be used as sensing devices[20]. For instance, Harbuzaru et al.[21] reported a new microporous lanthanide luminescent MOF, ITQMOF-1 and ITQMOF-2 (ITQMOF= Instituto de Technologia Quimica Metal Organic Frameworks), based on highly hydrophobic organic ligand HFIPBB. In the presence of water, these MOFs show no quenching of luminesce where as in the presence of ethanol enables them to sense ethanol in both air and water. It was also reported that the choice of Ln^{3+} metal is significant to the luminescent properties of the MOFs. Atomic structure, particle size, defects, and homogeneity in composition are all factors which affect the properties of luminescent materials[22].

Typically in luminescent MOF materials, a conjugated organic ligand behaves as luminescent linker, where emission directly involves a charge transfer with the coordinated metal ions. Lanthanide (Ln)-based luminescence is typically weakly emissive or often requires an "antenna" molecule to increase the sensitization of metal (figure 9). The mechanism of antenna sensitization within metal organic frameworks (MOFs) follows three steps: (1) energy is absorbed by the organic ligands around the lanthanide ions, (2) energy is transferred to the lanthanide ions from organic ligands, and (3) luminescence is generated from the lanthanide ions as shown in figure 8.

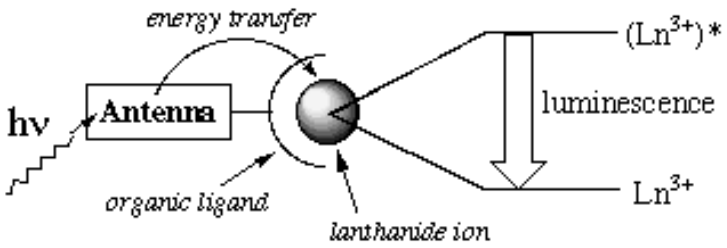

Figure 8 Antenna effect

The linker in luminescent Ln-MOFs is able to play this role through the transference of energy to the lanthanide (Ln) metal center. The antenna effect can be observed within a framework when a ligand molecule absorbs energy and transfers it to the metal center. The antenna effect can be used to probe the energy transfer within the MOF through the use of different organic ligands. π to π interaction between linkers or between a linker and a guest molecule can produce broad ranges of luminescence when comparing different complexes[23] due to the existence of a number of different rigid π–conjugated organic molecules. Organic linkers are stabilized within MOFs which reduces the nonradioactive decay rate. In addition, the size and nature of metal ions, the arrangement of the linkers, and the coordination environment within MOF can affect the luminescent properties of the organic linker due to different intermolecular and intramolecular interactions among organic linkers[17].

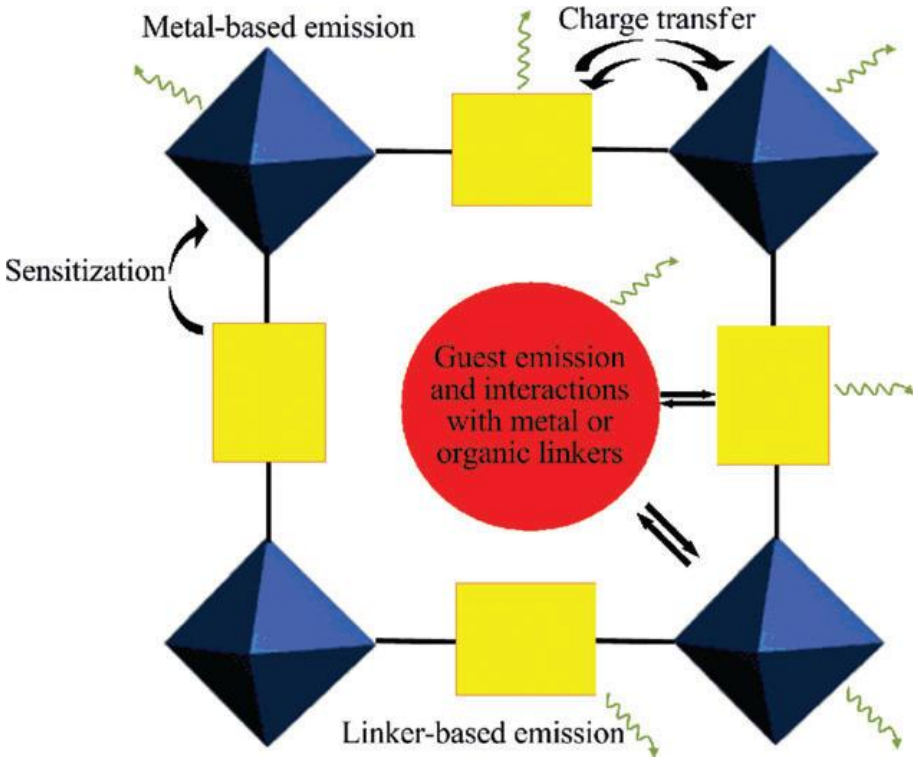

Figure 9 Representation of emission possibilities in a porous MOF, Wherein metal clusters (blue octahedra) are linked by organic linkers (Yellow rectangles) with an incorporated guest (red circle)[19]

Crosby and Wahn proposed the common energy migration paths from the conjugated ligand-center to the lanthanide ions where absorptions followed by intersystem crossing S_1-T_1, T_1-Ln^{3+} transfer, and metal-centered emission. This scheme can be modeled using Jablonski diagrams shown in Figure 10. Another path is the direct transfer of energy from the excited singlet state S_1 to the energy levels of the lanthanide ion, which is known for Eu^{3+} and Tb^{3+},[24]

.

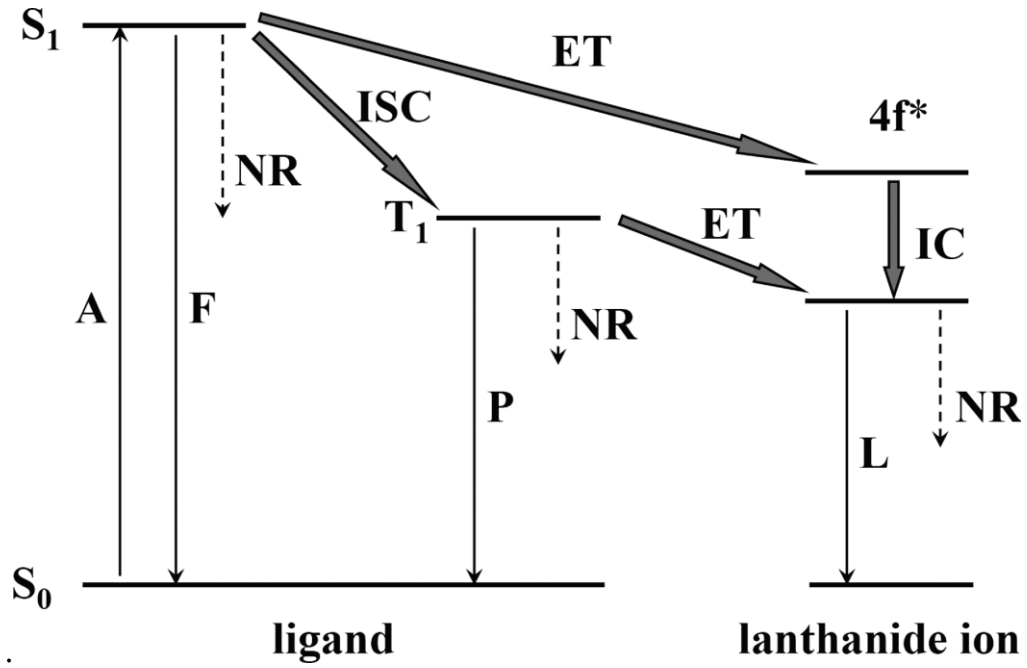

Figure 10 Schematic representation of photophysical processes in lanthanide (III) complexes (antenna effect). Abbreviations: A) absorption; F) fluorescence; P) phosphorescence; L) lanthanide- centered luminescence; ISC) intersystem crossing; ET) energy transfer; S) singlet; T) triplet. Full vertical lines indicate radiative transitions; dotted vertical lines indicate nonradiative transitions.

The antenna effect only occurs if the triplet state of the organic linker is located near energy level of the lanthanide ions. Therefore it is very important to design or choose suitable organic linkers to be used in luminescent MOFs materials.

These materials are attractive for a number of applications involving small molecule storage and delivery due to uptake of guests. Jaheon Kim et al.[25] reported mesoporous MOF derived from a superstructure of Tb(III) ions, triazine-1,3,5-(4,4',4''-trisbenzoate), and dimethylacetamide under elevated temperature and reduced pressure shown in figure 11, where the ferrocene-included framework. The inclusion of vapor phase ferrocence gives the color change to a dark brown and loss of Tb luminescence[25] and further suggests that the guest

ferrocene adds a non radiative energy-transfer pathway to quench the Tb emission. Due to the large pore sizes and small entryways, this material is attractive for a number of applications involving storage and delivery of small molecules. Under high temperature and vacuum, removal of guest ferrocene leads to the recovery of the framework luminescence.

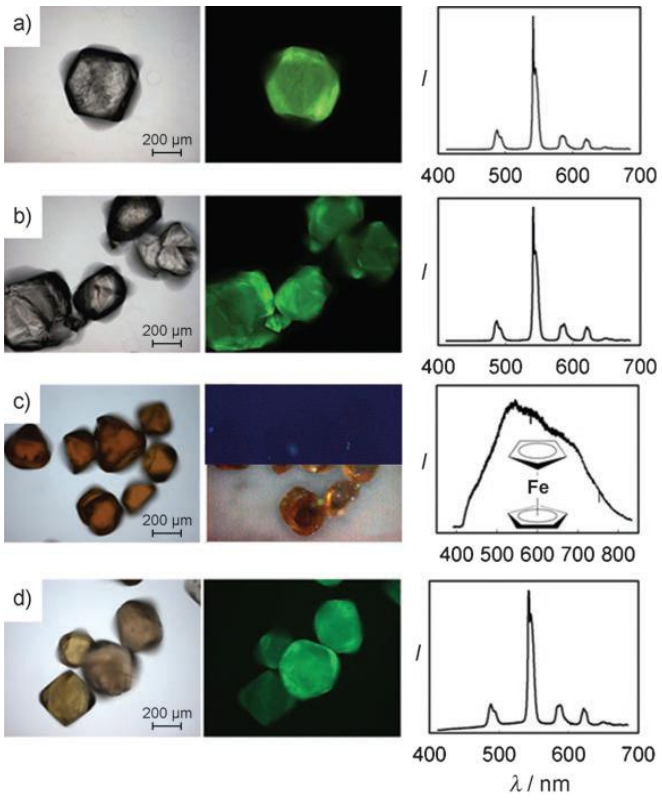

Figure 11 Transmission and fluorescence microscope images and luminescence spectra for (a) single crystal, (b) bulk, (c) ferrocene included, and (d) after removal of ferrocene of the MOF in part (a)[31].

IV. EXPERIMENTAL SECTION:

Synthesis:

Compounds **1, 2, 3,** and **4** were synthesized under solvothermal conditions using Teflon – Lined Parr stainless steel autoclaves shown in figure 12. Starting materials include erbium nitrate pentahydrate ($Er(NO_3)_3.5H_2O$, 99.9%, Alfa Products), terbium nitrate pentahydrate ($Tb(NO_3)_3.5H_20$, 99.9%, Aldrich), neodymium nitrate pentahydrate ($Nd(NO_3)_3.5H_20$, 99.9%, Alfa Products), dysprosium nitrate pentahydrate ($Dy(N0_3)_3.5H_20$, 99.99%, Reaction), Thiophene-2,5-dicarboxylic acid (2,5-TDC, $C_6H_4O_4S$, 97%, Sigma-Aldrich), ethanol (C_2H_5OH, 99%, Sigma-Aldrich) and distilled water (H_2O) and were used without any further purification.

Figure 12 Synthesis apparatus

Synthesis of 1 [$Tb_4(C_{44}S_6O_{37})$]

In a 23 ml Teflon liner, 1 mmole (0.435g) of $Tb(NO_3)_3.5H_20$ and 1 mmole (0.172g) of 2, 5 TDC were dissolved in 8.62 grams of Ethanol and 3.35 grams of distilled water and stirred for 3 hours to achieve solubility [molar ratio of metal salt: ligand: ethanol : water = 1:1: 0.185: 0.187]. The Teflon liner was transferred to stainless steel autoclave and the resultant solution was heated for a period of 3 days at 105°C. After cooling to room temperature, the product was recovered by filtration and subsequently washed with ethanol and water.

Synthesis of 2 [$Dy_4(C_{46}H_{43}O_{32}S_6)$]

In a 23 ml Teflon liner, 1 mmole (0.438g) of $Dy(NO_3)_3.5H_20$ and 1 mmole (0.172g) of 2, 5 TDC were dissolved in 8.62 grams of Ethanol and 3.35 grams of distilled water and stirred for 3 hours to achieve solubility [molar ratio of metal salt: ligand: ethanol : water = 1:1: 0.185: 0.187]. The Teflon liner was transferred to stainless steel autoclave and the resultant solution was heated for a period of 3 days at 105°C. After cooling to room temperature, the product was recovered by filtration and subsequently washed with ethanol and water.

Synthesis of 3 [$Nd_2(C_{21}O_{16}S_4)$]

In a 23 ml Teflon liner, 1 mmole (0.420g) of $Nd(NO_3)_3.5H_20$ and 1 mmole (0.172g) of 2, 5 TDC were dissolved in 12 grams of Ethanol and stirred for 3 hours to achieve solubility [molar ratio of metal salt: ligand: solvent = 1:1: 0.260]. The Teflon liner was transferred to stainless steel autoclave and the resultant solution was heated for a period of 3 days at 105°C.

After cooling to room temperature, the product was recovered by filtration and subsequently washed with ethanol.

Synthesis of 4 [$Er_4(C_{16}O_{10}S_5)$]

In a 23 ml Teflon liner, 1 mmole (0.443g) of $Dy(NO_3)_3.5H_20$ and 1 mmole (0.172g) of 2, 5 TDC were dissolved in 8.62 grams of Ethanol and 3.35 grams of distilled water and stirred for 3 hours to achieve solubility [molar ratio of metal salt: ligand: ethanol : water = 1:1: 0.185: 0.187]. The Teflon liner was transferred to stainless steel autoclave and the resultant solution was heated for a period of 3 days at 105°C. After cooling to room temperature, the product was recovered by filtration and subsequently washed with ethanol and water.

X-ray Crystallography

A suitable crystal of each compound **[1]**, **[2], [3],** and **[4]** was selected from the bulk samples and were mounted on a glass fiber using epoxy. Reflections for compound [**1**] **[2], [3],** were collected at ChemMatCars (Sector 15) at the Advanced Photon Source using a three-circle Bruker D8 diffractometer equipped with an APEXII detector at 100 K using synchrotron X-ray radiation (λ= 0.41328Å) and 0.5° φ scans. The raw intensity data were analyzed using the APEXII [26] suite of software at which time it was determined that the crystal contained more than one component. Cell_now [27] was used to determine the non-merohedral twin law [1 0 0 0 -1 0 -0.381 0 -1] relating the two major components by a 180.0° rotation about the 'a' axis. The data were then integrated using two components and were corrected for absorption using TWINABS[28]. The major component contained 38% of the sample intensity. The structure was

solved using direct methods and was refined using SHELXL[29]. All non-hydrogen atoms were refined anisotropically with the hydrogen atoms placed in idealized positions.

Reflections for compound **[4]** were collected using a Bruker four circle P4 single crystal diffractometer equipped with a SMART 1K CCD detector at room temperature (298K) using Mo Kα radiation (λ = 0.71073 Å) and φ and ω scans. The raw intensity data for compound **[2]** were collected and integrated with software packages, SMART[30] and SAINT[31]. An empirical absorption correction was applied using SADABS[28]. The crystal structure was solved using direct methods (SHELXS)[29]. All non-hydrogen atoms were refined anisotropically and the hydrogen atoms were added to the biphenyl rings using geometrical constraints (HFIX command).

Bulk sample identification and phase purity were determined using powder X-ray diffraction. The data were collected using a Scintag Pad-X diffractometer equipped with Cu Kα (λ = 1.5405 Å) radiation within a range of $5° \leq 2\theta \leq 40°$ (step size: 0.02°, counting time: 1s/step). Comparison of the observed and calculated powder X-ray diffraction patterns for **[1], [2],** and **[3]** confirmed phase purity, whereas PXRD for the compound **[4]** shows a small amount of impurity in structure shown in supplementary figures.

Thermal Data

Combined TGA-DSC data of **1, 2, 3,** and **4,** collected using a STA 449 C Jupiter Netzch Instrument are shown in figures 23-26 respectively. Powder samples were placed in an Al_2O_3

crucible for TGA-DSC and analyzed using a range of 30-650 °C and 5 degrees per minute temperature ramp under N_2 atmosphere.

Photoluminescence

Powder samples of **1, 2, 3,** and **4** and the free organic linker were analyzed at room temperature on a Fluorolog-3 with a 10 s integration time using an excitation wavelength of 397 nm.

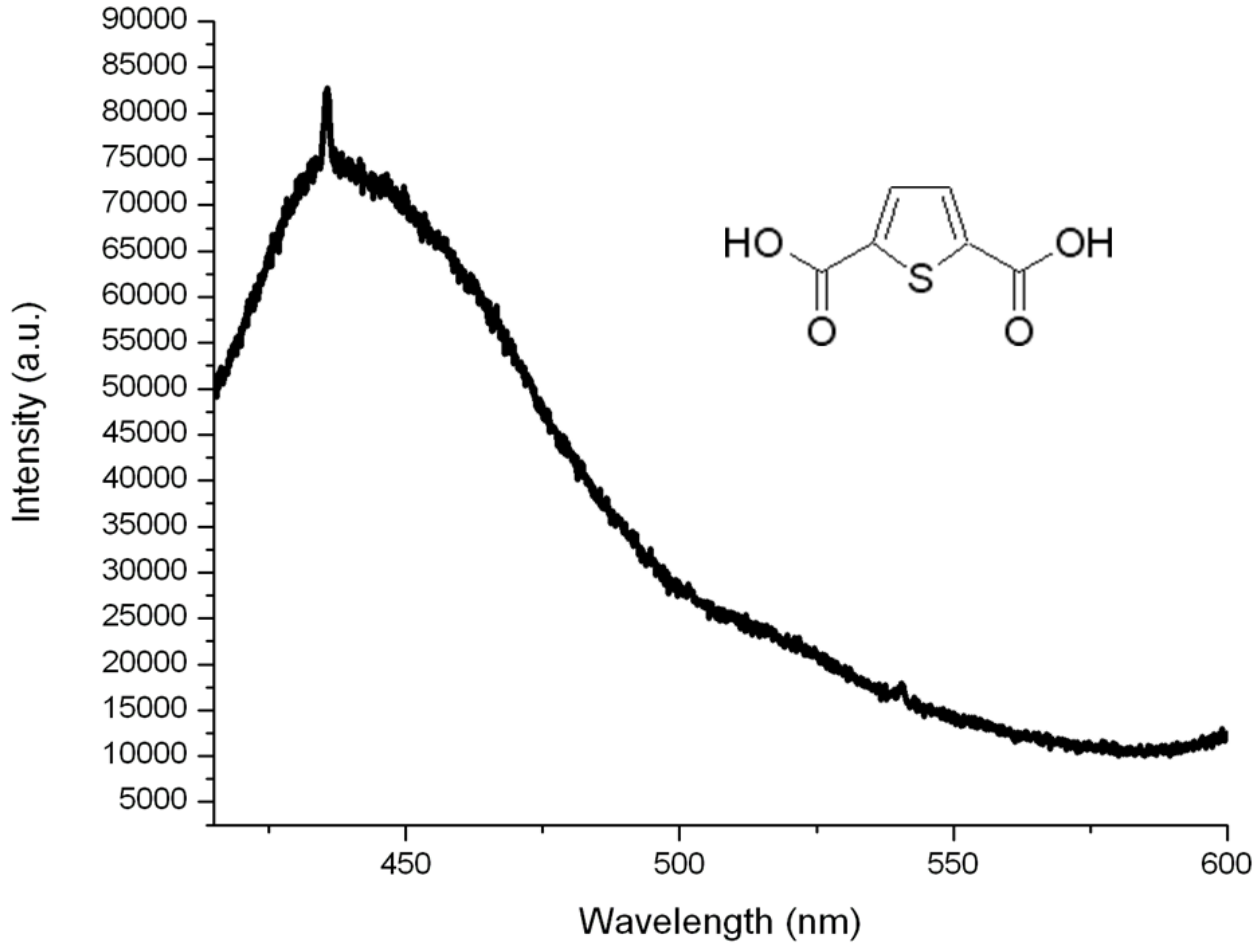

Figure 13 Luminescent spectra of Thiophene-2,5-dicarboxylic acid (free H_2TDC)

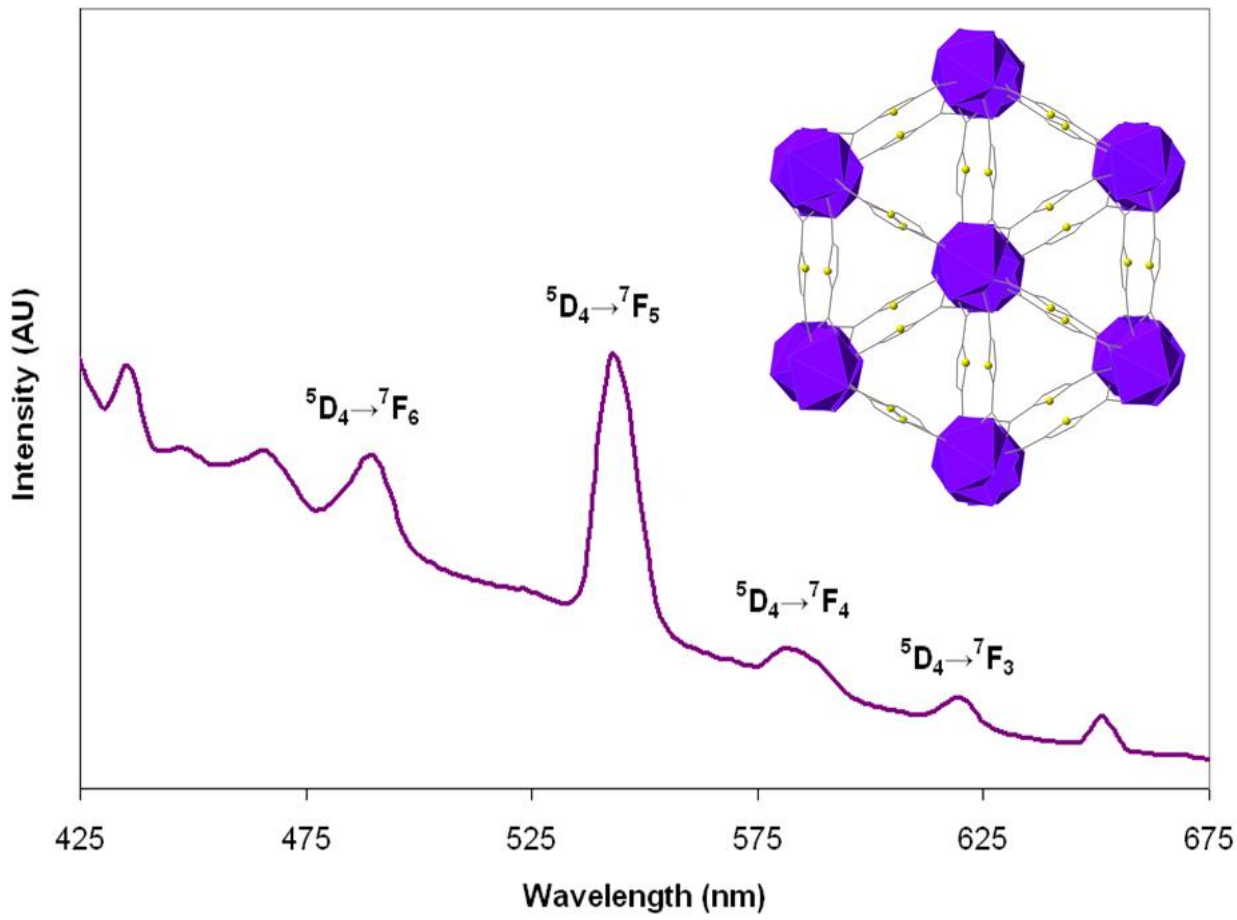

Figure 14 Structure of Tb_2 $(TDC)_3$ and Luminescent Spectra associated with it.

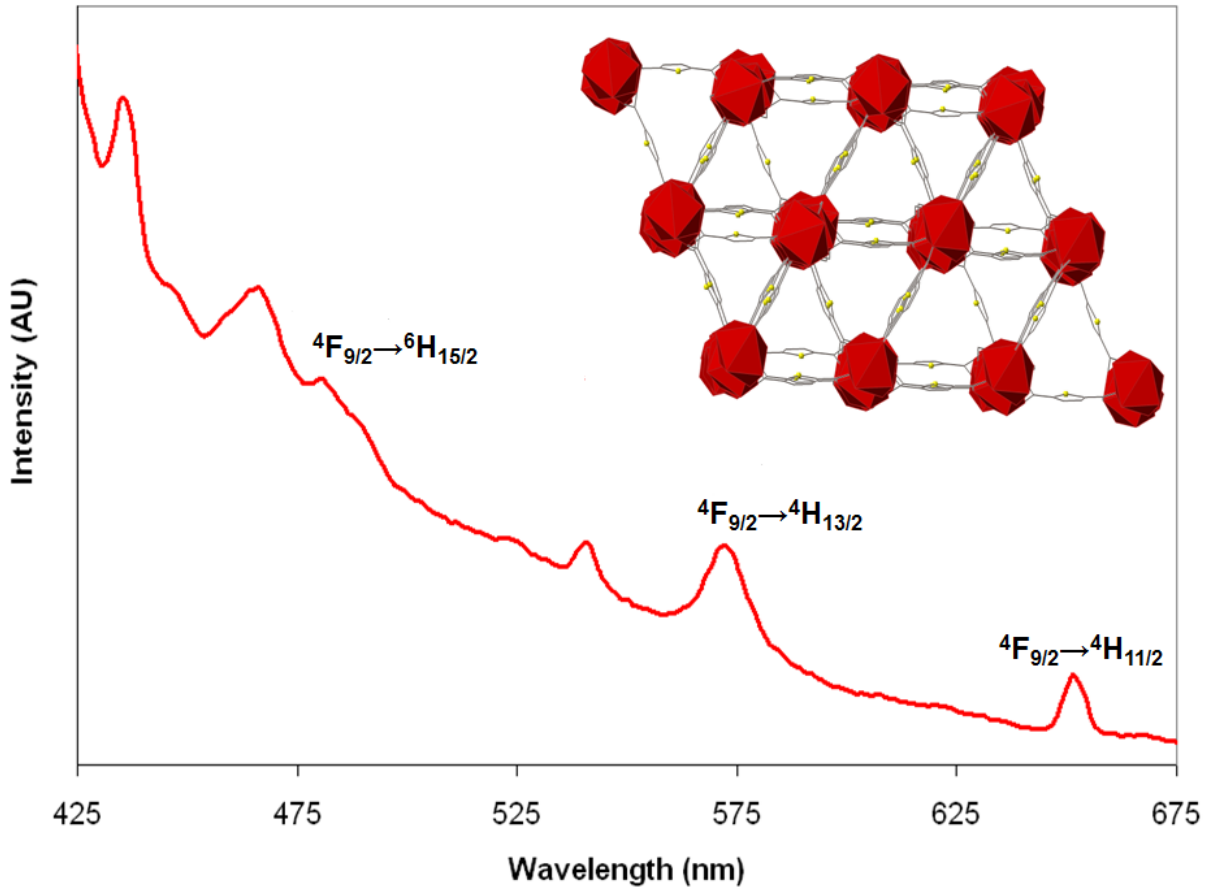

Figure 15 Structure of Dy_2 $(TDC)_3$ and Luminescent Spectra associated with it.

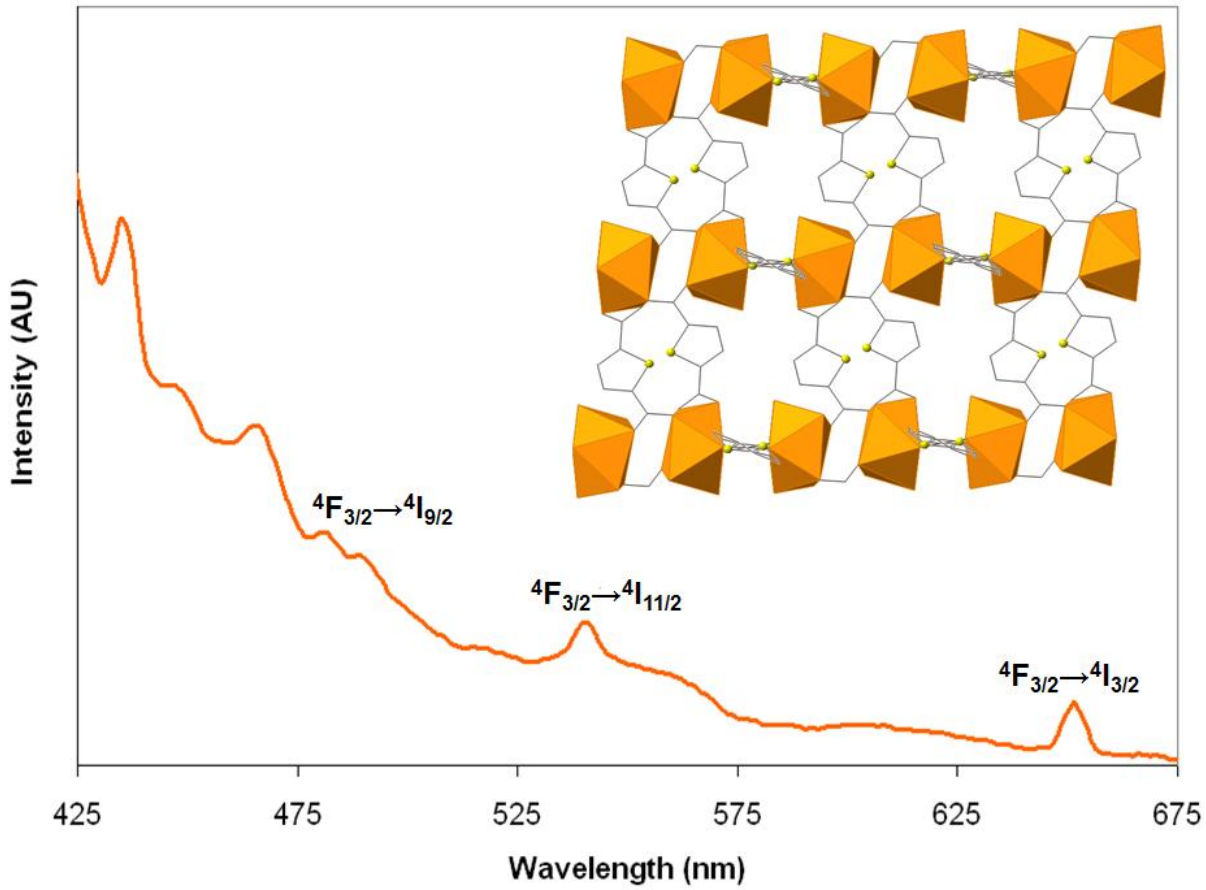

Figure 16 Structure of Nd_2 $(TDC)_3$ and Luminescent Spectra associated with it.

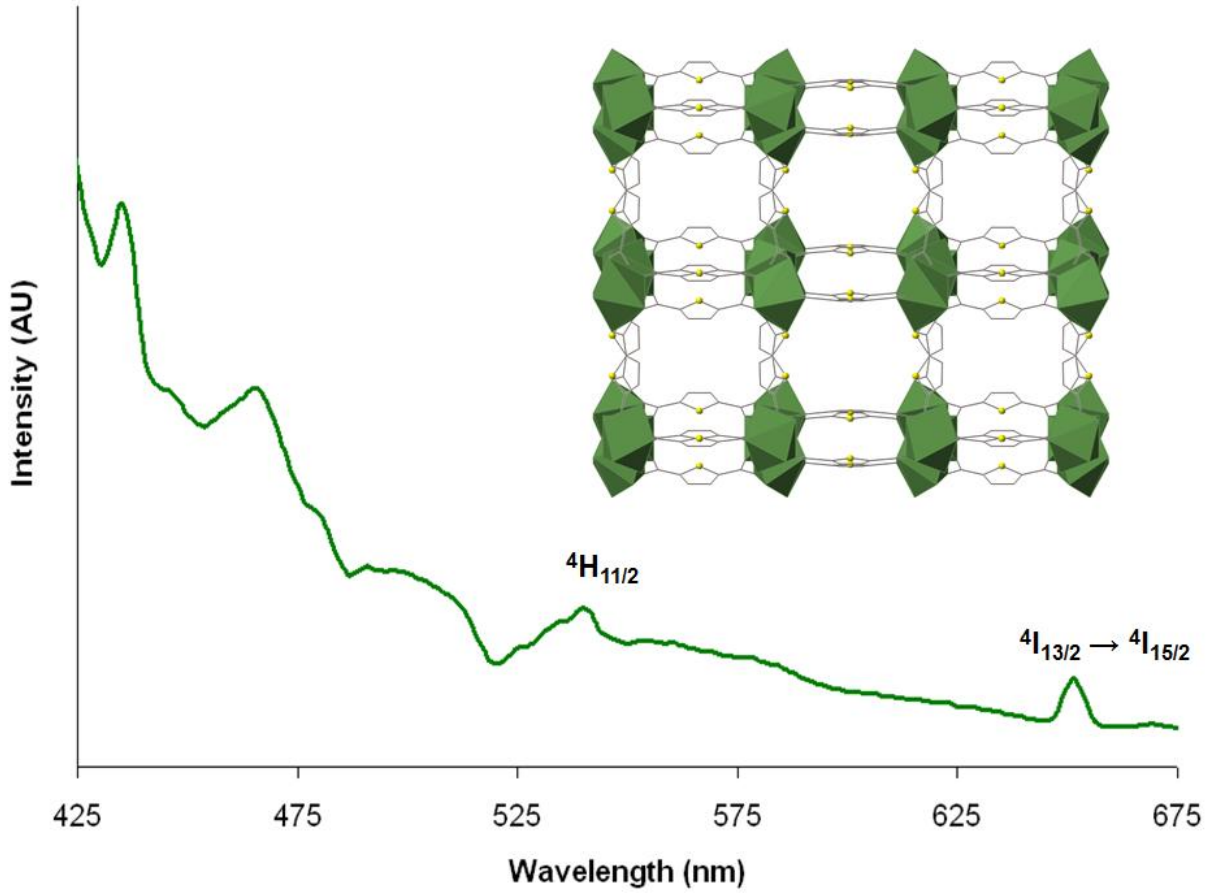

Figure 17 Structure of Er_2 $(TDC)_3$ and Luminescent Spectra associated with it.

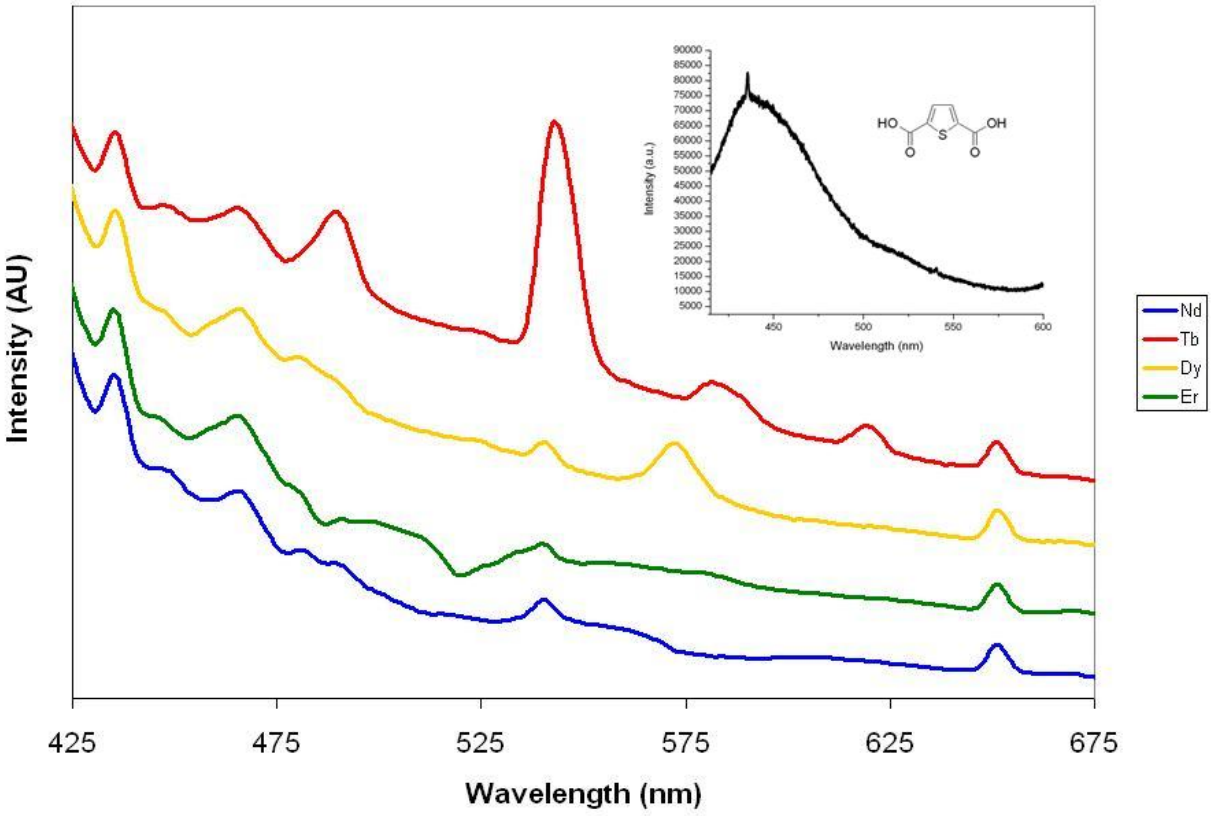

Figure 18 Combined Luminescent Spectra associated with TDC excitation at 397nm

V. DISCUSSION:

By varying the synthetic conditions such as temperature and solvents of the reaction, and holding the constant ratio of the metal-to-ligand, four new lanthanide thiophenedicarboxylate compounds are produced using thiophence-2,5-dicarboxylic acid (2,5 TDC) as an organic linker. The reactions of lanthanide nitrates (Tb, Dy, Nd, Er) and the organic linker 2,5 TDC in ethanol/water mixture forms compound **1, 2, 4** while compound **3** forms in ethanol solution. Compounds **1 – 4** have the similar structural, in which lanthanide ions act as a 5-connected nodes and the organic ligand acts as 4-connected nodes as shown in figure 14-7 respectively. Single crystal analysis shows that **1, 2,** and **4** are neutral 3D coordination polymers. The structure consists of an 8-coordinated Ln^{3+} (Ln^{3+} = Tb, Dy, Nd, Er) center, one and one-half of a 2,5 TDC ligands, and two coordinated water molecules in asymmetric unit. The tdc ligand is located on the 2-fold axis, as the Ln^{3+} metal center and water molecules are in general position. Each lanthanide (Tb, Dy, Nd, Er) are eight coordinated with eight oxygen atoms from two water molecules (O1w and O2w), four bidentate carboxyl group. Compound **3** forms in EtOH and is similar to **1, 2,** and **4** in that it also has its solvent molecules of EtOH coordinating to the metal center and also the coordinate metal center. Symmetry related Ln^{3+} ions are bridged by three carboxylate groups to form a triangular arrangement, which is extended with shared edges, and further connected by aromatic TDC linker and expand in crystallographic axes to form 3D network with three interpenetrated channels along the three crystallographic axes (figures 14-17). Increasing the composition of TDC in the compounds would benefit efficiently sensing the light for the hybrid to yield greater luminescence.

The thermogravimetric analysis (TGA) data shows that compounds **1, 2, 3,** and **4,** each undergo two distinct weight losses on heating in N_2 atmosphere. The first weight loss in the temperature range of 210-290 °C, 120-210 °C, 130-210 °C, and 130-170 °C for compounds **1, 2, 3,** and **4** (fig. 23-26) respectively. The release of solvent up to a high temperature is ascribed to the strong hydrogen bonding interaction with a descending trend following the lanthanide contraction. A further sharp weight loss was observed from 430 to 540 °C, where the pyrolysis of ligand occurs.

Photoluminescent (PL) analysis of lanthanide networks can provide more insight with the nature of metal-linker interaction. The luminescent of lanthanide inorganic – organic materials are currently drawing significant attention in the development of fluorescent materials. Therefore it is important to have systematic investigation of the photoluminescence with regards to the lanthanide coordination compounds. Excellent luminescent properties of Tb(III), and Dy(III) ions, are presented with the excitation of TDC ligand. The luminescence emission spectra of terbium compound is determined on excitation at 397 nm the Tb(III) emission spectra of this compound is shown in figure 14. As expected, the four emission bands in the region of 475–495, 538–562, 576–584, and 615–624 nm are attributed to the characteristic emissions of Tb emissive state $^5D_4$ to the ground state ^7F_J (J = 6 → 3) respectively. The luminescent spectra are dominated by the $^5D_4 \rightarrow {}^7F_5$ transitions in the range of 538–552 nm which create the most intense green luminescence output spectra for the solid sample. With regards to the luminescence spectra of dysprosium compound, the Photoluminescence was analyzed under excitation of 397 nm and shown (figure 15). In the photoluminescence spectrum, three emission bands at 474-477, 569-577, and 653-669 nm indicate the characteristic behaviors of Dy^{3+} ions,

which are assigned to $^4F_{9/2} \rightarrow {}^6H_J$ (J = 15/2, 13/2, and 11/2) transitions, respectively. Strong emission bands in the region of 474–477 nm are assigned to the blue insensitive transitions $^4F_{9/2} \rightarrow {}^6H_{15/2}$, whereas the more intensive emission bands in the range of 569–577 nm belongs to the yellow sensitive transitions $^4F_{9/2} \rightarrow {}^6H_{13/2}$ of dysprosium ions. The much weaker emission bands in the region of 653–669 nm in these polymers correspond to the $^4F_{9/2} \rightarrow {}^6H_{11/2}$transitions. In these dysprosium coordination compounds, the wide emission bands in the region of 360–460 nm are ascribed to the linker TDC transition, indicating that the energy is not fully transferred from the linker TDC to Dy ions. The luminescent property of Nd^{3+} compound was excited at 397nm which gives three emission bands at λ=477, 542, and 650 nm (figure 16), which are assigned to the $^4F_{3/2} \rightarrow {}^4I_{9/2}$, $^4F_{3/2} \rightarrow {}^4I_{11/2}$, and $^4F_{3/2} \rightarrow {}^4I_{3/2}$ transitions, respectively. The strongest emission is observed at the transition $^4F_{3/2} \rightarrow {}^4I1_{1/2}$ of 544 nm, and the emissions at $^4F_{3/2} \rightarrow {}^4I_{9/2}$ and $^4F_{3/2} \rightarrow {}^4I_{9/2}$ are weaker, which are in agreement with other reported results[32]. The luminescent spectra of Er^{3+} shows two bands at λ = 540 and 651 (figure 17) which are assigned to the $^4H_{11/2}$ and $^4I_{13/2} \rightarrow {}^4I_{15/2}$. The literature reveals that the visible emissions in the range of 600-720 nm of all of the complexes exhibit quite fast decay times (i.e., shorter than 1 μs)[33]. This is particularly relevant in comparison with the visible phosphorescence band $^4I_{13/2} \rightarrow {}^4I_{15/2}$. Figure 18 shows the luminescence of all the compounds with respect to the excitation of TDC.

VI. FUTURE PROSPECTS:

Future prospects will include the completion of single crystal XRD structures, DFT calculations, and CHN analysis of complexes compounds **[1], [2], [3],** and **[4].** Future work will be done by senior members in our group.

The synthesis of more lanthanides compounds with thiophene-2,5-dicarboxylic acid linker will be explored by varying solvents and temperature.

VII. CONCLUSION:

Four new 3D lanthanide thiophenedicarboxylate frameworks had been synthesized and characterized using identical metal-to-linker ratios. The TDC ligand plays a versatile role in these compounds towards different lanthanide ions to form 3-D inorganic-organic hybrid frameworks. The differences in the framework topologies arise when either ethanol or water are used a reaction solvents. Crystal structure of the compounds and corresponding luminescent properties are presented here. Compounds were excited at 397 nm. $Tb_2(TDC)_3$ shows the most intense emission of the three compounds. These findings offer a better understanding of how linker choice can affect luminescent properties of resulting coordination networks. The success in production of complexes **1 – 4** indicates that the lanthanide ions can be powerful building blocks to construct attractive MOFs with novel topologies.

VIII. SUPPLIMENTARY FIGURES:

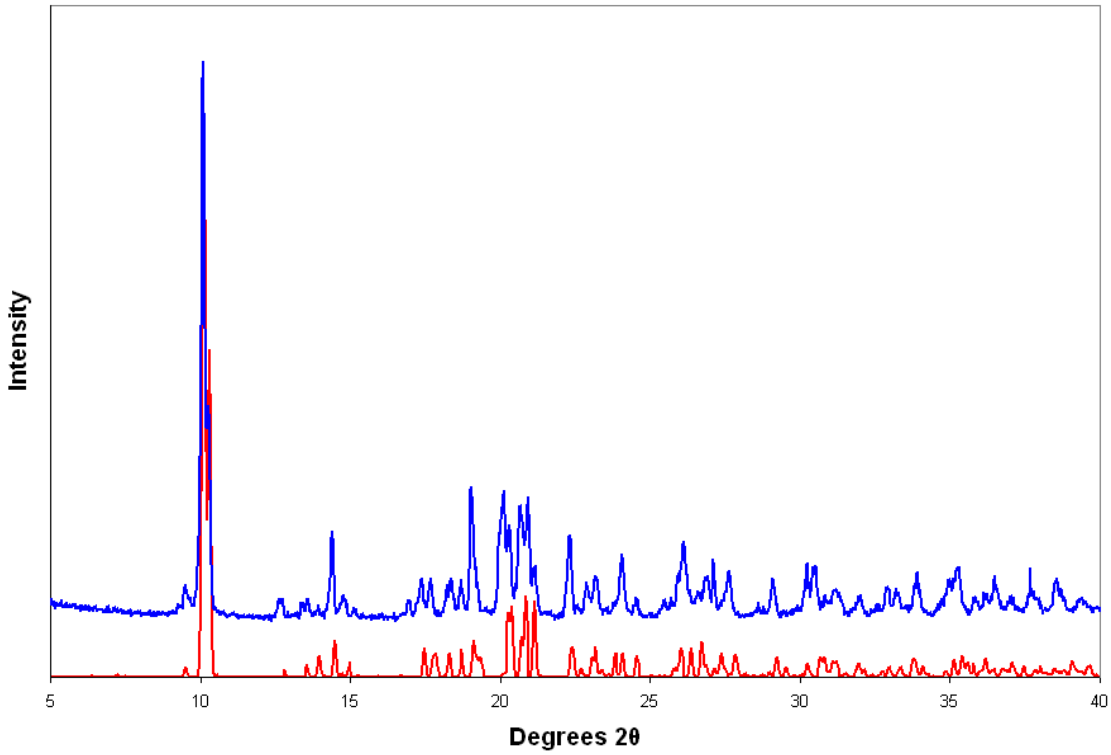

Figure 19 The simulated (red) and experimental (blue) PXRD of Compound **1**

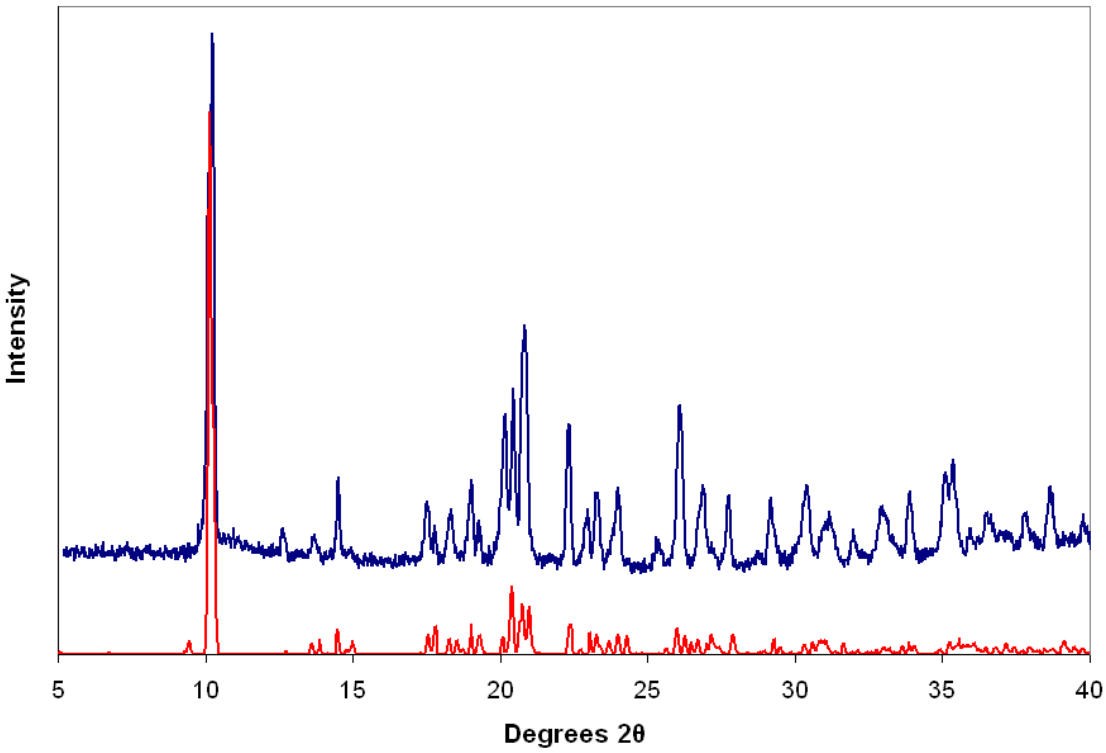

Figure 20 The simulated (red) and experimental (blue) PXRD of Compound **2**

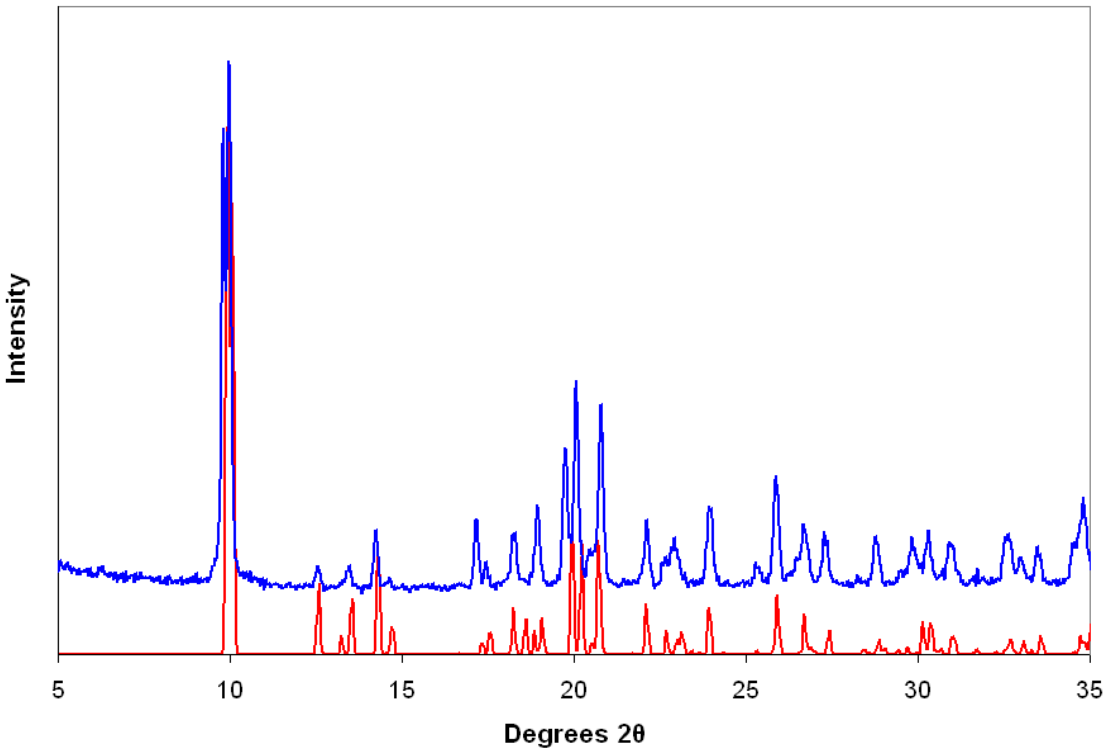

Figure 21 The simulated (red) and experimental (blue) PXRD of Compound **3**

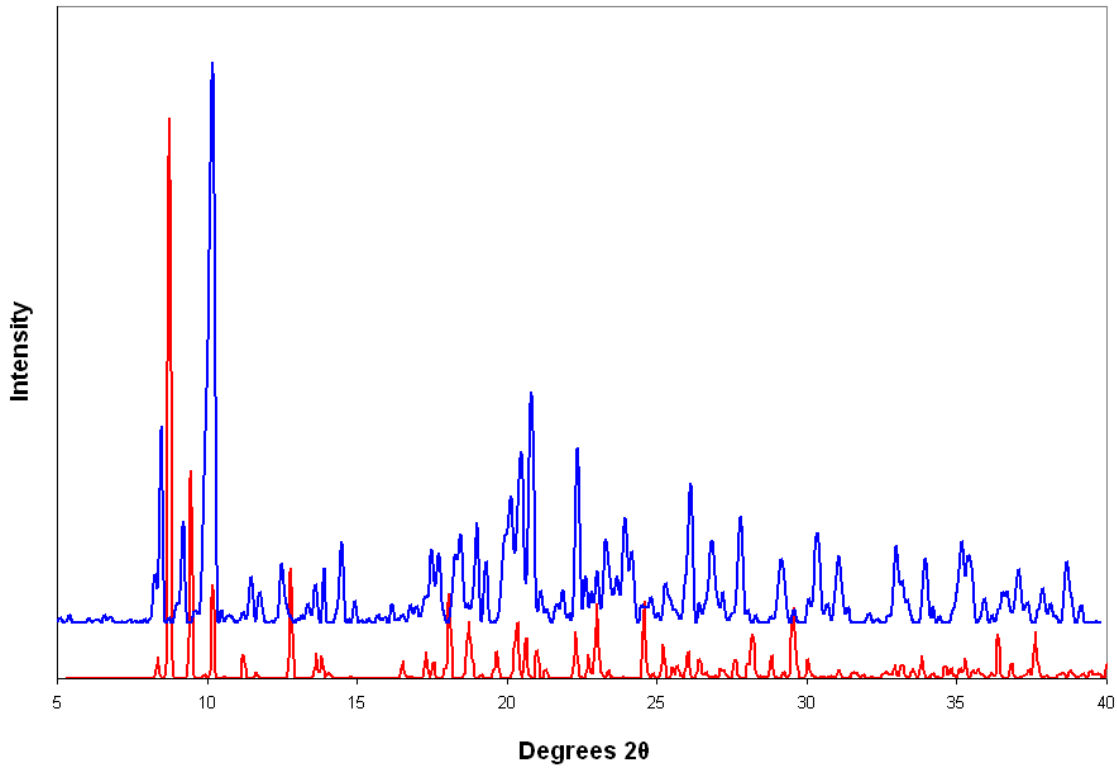

Figure 22 The simulated (red) and experimental (blue) PXRD of Compound **4**

TGA-DSC of $Tb_2(TDC)_3$

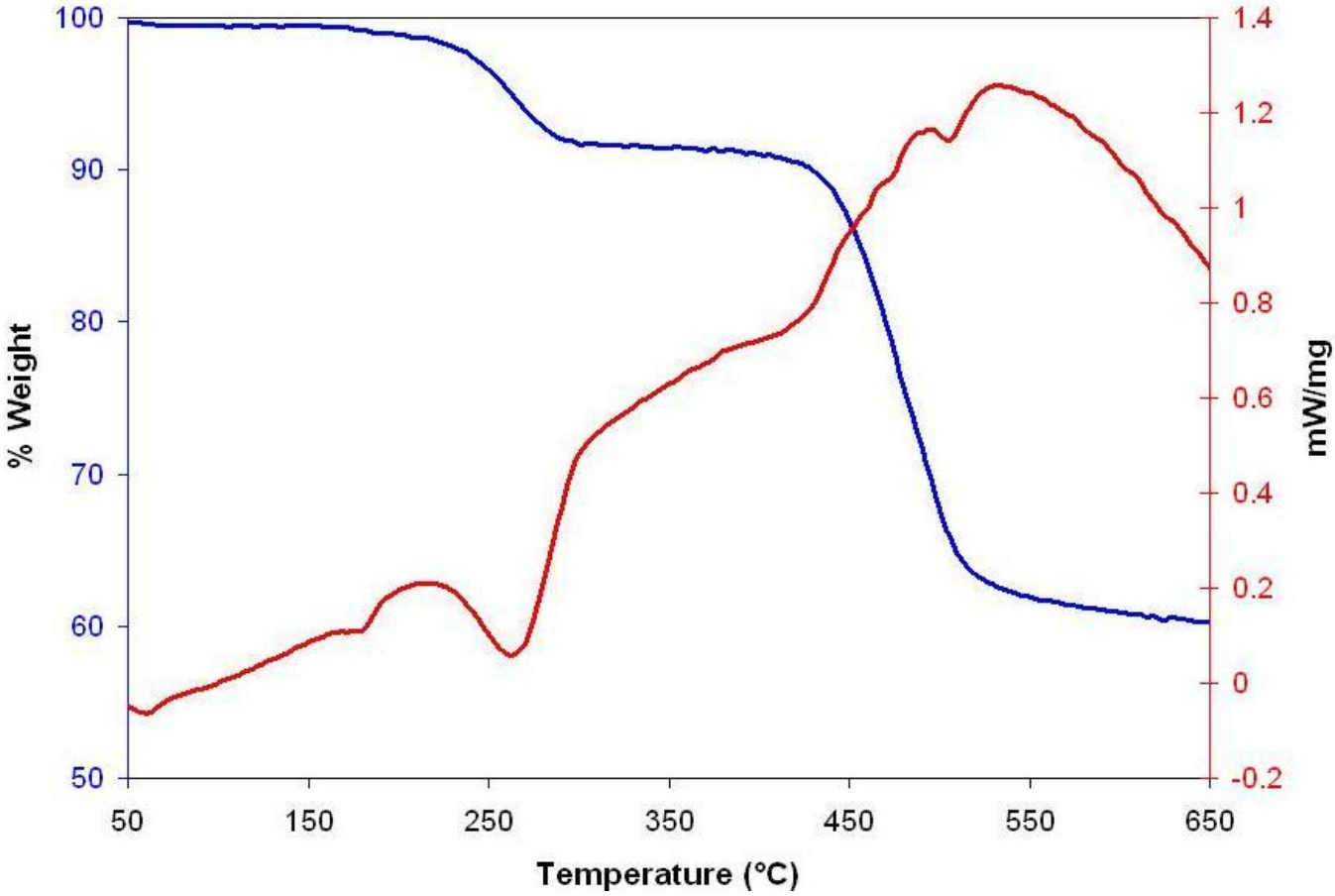

Figure 23 TGA-DSC of $Tb_2(TDC)_3$. The blue line represents TGA plot, while the ref line shows the DSC signal associated with it.

TGA-DSC of $Dy_2(TDC)_3$

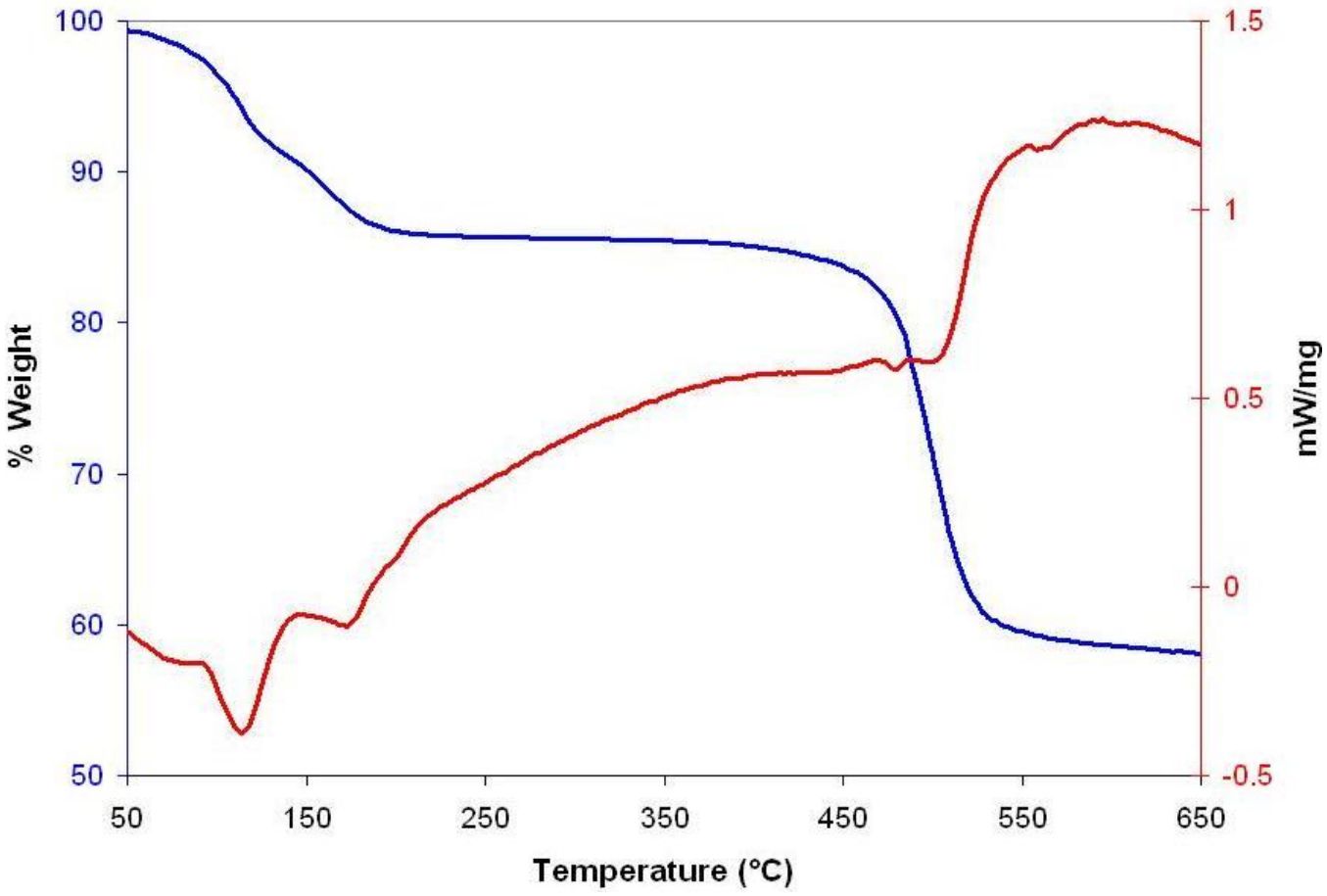

Figure 24 TGA-DSC of $Dy_2(TDC)_3$. The blue line represents TGA plot, while the ref line shows the DSC signal associated with it.

TGA-DSC of $Nd_2(TDC)_3$

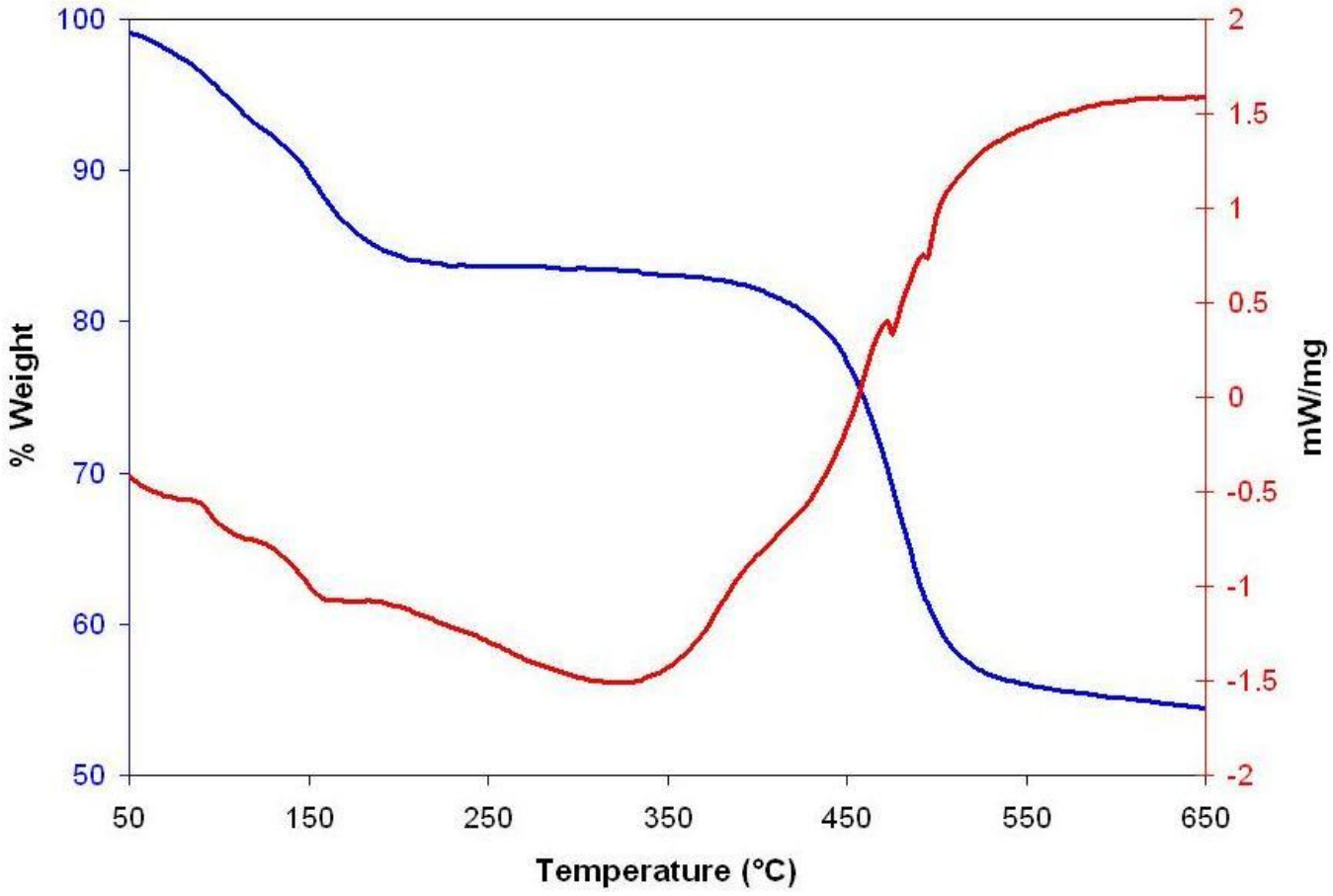

Figure 25 TGA-DSC of $Nd_2(TDC)_3$. The blue line represents TGA plot, while the ref line shows the DSC signal associated with it.

TGA-DSC of $Er_2(TDC)_3$

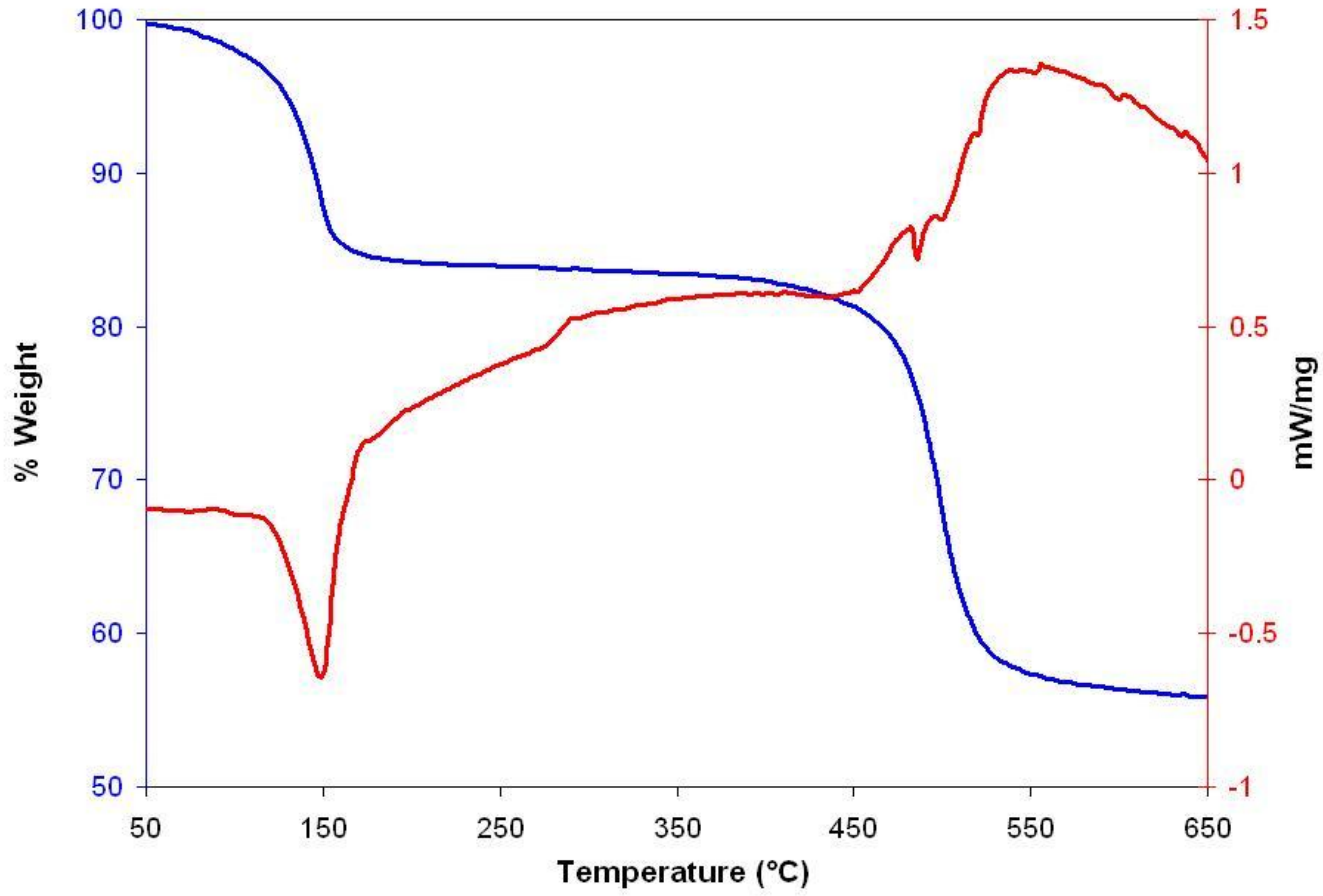

Figure 26 TGA-DSC of $Er_2(TDC)_3$. The blue line represents TGA plot, while the ref line shows the DSC signal associated with it.

REFERENCES:

1- (a)Eddaoudi,M ; Kim, J.; Rosi, N.; Vodak D.; Wacheter,J.; O'Keeffe, M.; Yaghi, O. M. *Science* **2002,** *295* (5554), 469.

(b)Rowsell, J. L. C.; Yaghi, O.M. *Microporous Mesoporous Matter.* **2004,** *73*, 3.

2- Forster, P., M., Burbank, A.R., Livage, C., Ferey, G.,Cheetham, A., K., *Chem. Comm.,* **2004,** 368.

3- Zhang, J. ; Liu, R.; Feng, P.; Bu. X. *Angew. Chem. Int.* **2007,** *46*, 8388.

4- Liu, C. M.; Xiong, R. G.; You, X. Z.; Chen, W.; *Acta Chem. Scan.* **1998,** *52*, 135.

5- Maji, T K; Matsuda, R.; Kitagawa, S.; *Nat. Mater*. **2007,** *6*, 142.

6- Zhao, B.; Chen, X. Y.; Cheng, P.; Liao, D. Z.; Yan, S. P.; Jiang, Z. H. *J. Am. Chem Soc*. **2004**, *126*, 15394.

7- Poulsen, R. D.; Bentien, A.; Chevalier, M.; Iversen, B. B. *J. Am. Chem. Soc*. **2005**, *127*, 9156

8- Milward, A. R.; Yaghi, O. M. *j. Am. Chem. Soc*. **2005.** *127*, 17998.

9- Chen, B.; Liang, C.; Yang, J.; Contreras, D. S.; Clancy, Y. L.; Lobkovsky, E. B.; Yaghi, O. M.; Dai, S. *Angew. Chem. Int. Ed*. **2006**, *45*, 1390.

10- Serpaggi, F.; Luxbacher, T.; Cheetam, A. K.; Ferey, G., *J. Solid State Chem.* **1999,** *145*, 580.

11- (a) Read, C.; Petrovic, J.; Ordaz, G.; Satyapal, S. *Mater. Res. Soc. Symp. Proc*. **2006**, *885*, 125.

(b) Debasis, B.; Sun, J. K.; John, B. P.; *Crys. Growth Design*, **2009,** *9*, 2500.

12- (a) Long J. R., Yaghi O. M., *Chem. Soc. Rev*., **2009**, *38*, 1213-1214.

(b) Rowsell, J., L., C.,Yaghi, O., M., *Angew. Chem. Int. Ed.* **2005,** *44*, 4670-4679.

13- Wu, C. D.; Hu, A.; Zhang, L.; Lin, W. B. *J. Am. Chem. Soc.* **2005**, *127*, 8940.

14- J. R. Lakowicz, Principles of Fluorescence Spectroscopy, Springer, New York, 2006, 3rd edn.

15- Claude, J., Bunzli, G., Piget, C., *Chem. Soc. Rev*., **2005,** *24*, 1048.

16- Moore, E. G.; Samuel, A. P. S.; Raymond, K. N. Acc. Chem. Res.,**2009**, *42*, 542.

17- Binnemans, K. *Chem. Rev*. **2009**, *109*, 4283.

18- (a) Cahill, C. L.; de Lill, D. T.; Frisch, M. *CrystEngComm* **2007**, *9*, 15.

(b) Suh, M.; Cheon, Y.; Lee, E. Coord. *Chem. Rev*. **2008,** *252*, 1007.

(c) Maspoch, D.; Ruiz-Molina, D.; Veciana, *J. Chem. Soc. Rev*. **2007**, *36*, 770.

(d) Rocha, J.; Carlos, L. D.; Paz, F. A. A.; Ananias, D. *Chem. Soc. Rev.*, **2011**, *40*, 926.

(e) Allendorf, M. D.; Bauer, C. A.; Bhakta, R. K.; Houk, R. J. T., *Chem. Soc. Rev*. **2009**, *38*, 1330.

(f) Chen, B.; Xiang, S.; Qian, G. *Acc. Chem. Res*. **2010**, *43*, 1115.

(g) Meek, S. T.; Greathouse, J. A.; Allendorf, M. D. *Adv. Mater*., **2011**, *23*, 249.

(h) Shekhah, O.; Liu, J.; Fischer, R. A.; W€oll, C. *Chem. Soc. Rev*., **2011**, *40*, 1081.

(i) Ferey, G. *Chem. Soc. Rev*. **2008**, *37*, 191.

19- (a) Binnemans, K. *Chem. Rev*. **2009**, *109*, 4283.

(b) Hwang, S. H.; Moorefield, C. N.; Newkome, G. R. *Chem. Soc. Rev*. **2008**, *37*, 2543.

20- Achmann, S., Hagen, G., Kita, J., Malkowsky, I. M., Kiener, C., Moos, R. **2009,** *9*, 1574-1589.

21- Harbuzaru, B.,V., Corma, A., Rey, F., Atienzer, P., Lorda, J., L., Garcia, H., Ananias, D., Carlos, L.D., Rocha, J., *Angew. Chem. Int. Ed.* , **2008,** *47*, 1080-1083..

22- Cui,Y., Yue, Y., Qian, G., Chen, B., *ACS ASAP*.

23- Allendorf, M. D., Bauer, C. A., Bhaka, R., Houk, R. J. T., *Chem. Soc. Rev.* **2009**, *38*, 1330.

24- Moore, E. G.; Samuel, A. P. S.; Raymond, K. N. Acc. *Chem. Res*., **2009**, *42*, 542.

25- Y. K. Park, S. B. Choi, H. Kim, K. Kim, B. H. Won, K. Choi, J. S. Choi, W. S. Ahn, N. Won, S. Kim, D. H. Jung, S. H. Choi, G. H. Kim, S. S. Cha, Y. H. Jhon, J. K. Yang and J. Kim, *Angew. Chem*., Int. Ed., **2007**, 46, 8230–8233.

26- APEXII *APEX II*, v.2009.3-0; Bruker AXS, Inc.: Madison, Wisconsin, USA, **2009**.

27- Sheldrick, G. M. *CELL_NOW*, 2008/2; Bruker AXS: Madison, WI, **2008**.

28- Sheldrick, G. M. *TWINABS*, 2008/2; Bruker AXS: Madison, WI, **2008**.

29- Sheldrick, G. M., *Acta Crystallogr, Sect. A: Found. Crystallogr*. **2008,** *64*, 112.

30- SMART, 5.6; Bruker-AXS: Madison, WI **2001**.

31- SAINT 5.1; Bruker-AXS: Madison, WI **2000**.

32- Dai, F. Cui, P., Fei Y., Sun, D, *Cryst.Growth Design*, **2010,** *10*, 1474.

33- Pizzoferrato, R., Francini, R., Pietrantoni, S., Paolesse, R., Mandoj, F., Monguzzi, A., Meinard, F., *J. Phy. Chem.*, **2010,** *114*. 4163-4168.